GRANT
N-05-CR
91532

TRAJECTORY OPTIMIZATION
FOR THE NATIONAL AEROSPACE PLANE

P.46

FINAL REPORT

May 1, 1991–May 30, 1992

June, 1992

Principal Investigator: Ping Lu

Department of Aerospace Engineering and Engineering Mechanics

Iowa State University

Ames, IA 50011

ACKNOWLEDGEMENTS

TABLE OF CONTENTS

LIST OF SYMBOLS

C_D	Drag coefficient
C_L	Lift coefficient
C_T	Thrust coefficient
c	Command altitude
D	Aerodynamic drag
d	Down range distance (km)
g_o	Gravitational acceleration (9.81 m/sec)
H	Hamiltonian
h	Altitude
I_{sp}	Specific impulse
J	Performance index
k_i	Controller gain constants
L	Aerodynamic lift
m	mass (kg)
p_i	Adjont state variables
Q	Convective heating rate
$\dot{Q}$	Time derivative of Q
Q_{max}	Maximum allowable level of Q
q	Dynamic pressure
$\dot{q}$	Time derivative of q
q_{max}	Maximum allowable level of q
r	Radius from the center of the earth
S	Switching function
T	Thrust
t	Time
$\mathbf{u}$	Control vector
v	Velocity
$\mathbf{x}$	State vector
α	Angle of attack
β	Recipical of scale height of atmospheric density

ε	Thrust angle
ϕ	Fuel equivalence ratio
γ	Flight path angle
η	Throttle setting
μ	Gravitational parameter
θ	Down range polar angle
ρ	Atmospheric density
superscript $'$	Derivative with respect to θ
superscript $*$	Nominal values
subscript $_{o,f}$	Initial and final point

LIST OF FIGURES

1. INTRODUCTION

The primary objective of this research is to develop an efficient and robust trajectory optimization tool for the optimal ascent problem of the National AeroSpace Plane (NASP). Since the model of the aerospace plane is highly numerical data-driven, and very stringent flight path constraints must be imposed for the safety and operational reasons, it is felt that the existing trajectory optimization techniques either cannot handle this problem or do not offer a completely satisfactory solution in accuracy or efficiency. The issue of on-board guidance also motivates the research. Although the solution for the optimal trajectory may have to be generated off-line, it would be highly desired if some algorithm can be set up so that the actual flight information can be incorporated with the open-loop optimal solution in a feedback fashion to control the vehicle in real-time.

This report is organized in the following order to summarize the completed work: Section 2 states the formualtion and models of the trajectory optimization problem. An inverse dynamics approach to the problem is introduced in Section 3. Optimal trajectories corresponding to various conditions and performance indeices are presented in Section 4. Based on the accurate optimal solutions, a midcourse nonlinear feedback controller is develped in Section 5 to obtain significantly simplified yet very accurate optimal trajectories. The remarkabe performance of the inverse dynamics approach and the midcourse controller in guiding the aerospace plane in the presence of disturbances and uncertainties is demonstrated in Section 6. Section 7 discusses rocket-assisted ascent which may be beneficial when orbital altitude is high. The possibility of singular control of the rocket is examined. Feedback control laws for the rocket are derived by using the inverse dynamics concept. Finally, Section 8 recommends some future research aspects for the subject. Detailed discussions of some of the above topics can be found in Refs. [1–2].

2. MODELS AND PROBLEM FORMULATION

The model for the aerospace plane is adopted from Ref. [3], known as the "Langley Accelerator". It is a generic model of a hypersonic vehicle with winged-cone configuration. The present study is restricted to two-dimensional motion. The motion is controlled by propulsion throttle and angle of attack which in turn affects the aerodynamic forces. The propulsion system is assumed to comprise of only airbreathing engines for now. The thrust is modeled by

$$T = C_T q$$

where q is the dynamic pressure, and C_T is the thrust coefficient. C_T and the specific impulse I_{sp} are given in tabular form as functions of Mach number, dynamic pressure and fuel-equivalence ratio, designated by ϕ. Equivalence ratio of unity corresponds to maximum fuel efficiency, and values greater than unity give more thrust but use disproportionately more fuel. Assuming a spherical, nonrotating earth and Newtonian gravitational field with $g = \mu/r^2$, the point mass equations of motion for the aerospace plane are

$$\frac{dr}{dt} = v \sin \gamma \tag{1}$$

$$\frac{d\theta}{dt} = \frac{v \cos \gamma}{r} \tag{2}$$

$$\frac{dv}{dt} = \frac{T \cos(\alpha - \varepsilon) - D}{m} - \frac{\mu \sin \gamma}{r^2} \tag{3}$$

$$\frac{d\gamma}{dt} = \frac{T \sin(\alpha - \varepsilon) + L}{mv} + \left(\frac{v}{r} - \frac{\mu}{vr^2}\right) \cos \gamma \tag{4}$$

$$\frac{dm}{dt} = -\frac{T}{g_0 I_{sp}} \tag{5}$$

In above equations, r is the radius from the center of the earth to the vehicle; θ the polar angle; v the velocity; γ the flight path angle and m the total mass. T is the thrust and I_{sp} is the specific impulse of the propulsion system. α denotes the angle of attack. ε is the thrust vector angle and will be assumed to be constant or zero for airbreathing engines. L and D are aerodynamic lift and drag, respectively. The atmospheric density is assumed to be an exponential function of altitude,

$$\rho = \rho_0 e^{-\beta(r - r_0)}$$

where $r_0 = 6378$ km is the radius of the earth. The lift and drag coefficient C_L and C_D are also given as functions of Mach number and the angle of attack in tabulated data. For convenience of later application, C_L for the basic vehicle is accurately approximated by

$$C_L = C_{L0}\alpha + C_{L1}\alpha^3 \tag{6}$$

where C_{L0} and C_{L1} are functions of Mach number, obtained by least-squares fit to the tabulated data for given α, and then interpolated by cubic splines over Mach number. Figure 1 shows C_{L0} and C_{L1} as function of Mach number. C_T, C_D and I_{sp} are interpolated using a multi-dimensional table look-up scheme.

The horizontal takeoff conditions from a runway at sea level are specified by initial velocity of Mach 0.5 and takeof mass of 133,809 kg (295,000 bf). Final orbit injection into a circular orbit at altitude h_c is achevied by constraining the terminal altitude $h(t_f)$, velocity $v(t_f)$ and flight path angle $\gamma(t_f)$

$$\begin{aligned} h(t_f) &= h_c \\ v(t_f) &= \sqrt{\frac{\mu}{r_0 + h_c}} \\ \gamma(t_f) &= 0 \end{aligned} \tag{7}$$

where the final time t_f is free. Two operational constraints on the trajectory are

$$q \le q_{max} \tag{8}$$

$$Q \le Q_{max} \tag{9}$$

where Q is the convective heating rate at the stagnation point. The optimization is to be performed with respect to the control variable ϕ and α so as to minimize the fuel consumption of the ascent trajectory, or, equivalently,

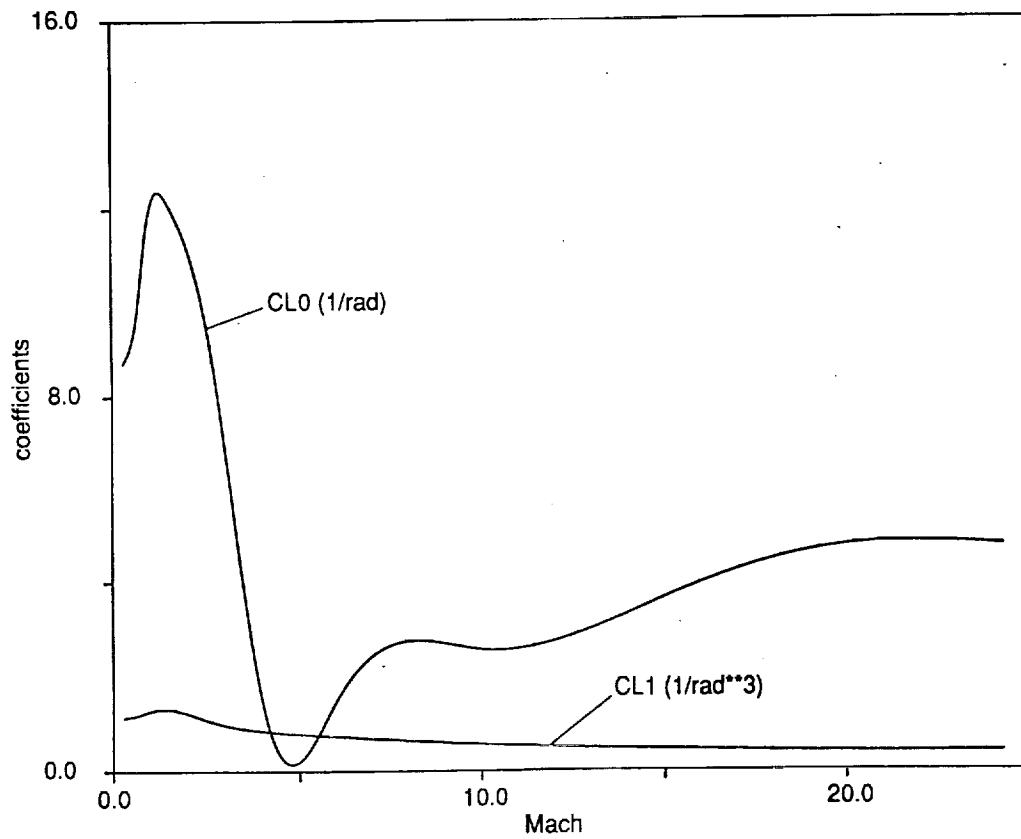$$\max_{\phi,\ \alpha}\ m(t_f)$$

3

Figure 1. Model of the lift: $C_L = C_{L0}\alpha + C_{L1}\alpha^3$

3. AN INVERSE DYNAMICS APPROACH

A representitive of the previous work is documented in Ref. [4] in which a singular perturbation method is utilized to analyze the near-optimal trajectory. Since no analytical functional forms of the system parameters C_D, C_T and I_{sp} are readily available for our aerospace plane model, and the problem is strongly nonlinear, a direct method using nonlinear programming approach appears to be more advantageous for accurate solutions. But it was found that the optimization problem is very poorly conditioned. This is mainly because the aerospace plane flies at hypersonic speeds, and any slight variations of controls will cause large perturbations in the trajectory down stream. This high sensitivity problem makes even the conventional direct approach not convergent in which the control histories, $\alpha(t)$ and $\phi(t)$, are directly parametrized. Early attempt to generate optimal trajectories succeeded only when no constraints (8) and (9) were enforced, becuase the unconstrained trajectory accelerates through the dense atomsphere very rapidly (within 3 minutes, the altitude is already 42 km, and the velocity reaches Mach 20). Clearly the unconstrained trajectory will not be feasible. To circumvent this difficulty, an inverse dynamics approach is introduced. The inverse dynamic problem (IDP) can be formally stated as the following:

Consider a dynamic system

$$\dot{\mathbf{x}} = \mathbf{f}(\mathbf{x}(t), \mathbf{u}(t), t) \tag{10}$$

with given initial conditions and terminal constraints

$$\mathbf{x}(t_0) = \mathbf{x}_0 \tag{11}$$

$$\mathbf{S}(\mathbf{x}(t_f), t_f) = 0 \tag{12}$$

Find a control $\mathbf{u}(t)$ such that the solution of (10) with initial condition (11) satisfies (12) and the given algebraic constraint

$$\mathbf{g}(\mathbf{x}(t), \mathbf{c}(t), t) = 0, \quad t \in [t_0, t_f] \tag{13}$$

where $\mathbf{g} : \mathbf{R}^n \times \mathbf{R}^m \times R \rightarrow \mathbf{R}^l$ is sufficiently differentiable. $\mathbf{c}(t) \in \mathbf{R}^m$ for $t_0 \leq t \leq t_f$ is a given smooth function. $\mathbf{c}(t)$ usually represents the desired output and (13) specifies the

output relationship. By repeatedly differentiating each component of (9) till **u** appears explicitly, we have additional constraints

$$\mathbf{G}(\mathbf{x}(t), \mathbf{u}(t), \mathbf{c}(t), \dot{\mathbf{c}}(t), ..., t) = 0 \qquad (14)$$

Equations (13) and (14) are the constraints on the state variables and controls. The existence of solution to such an inverse dynamic problem can be guaranteed under certain conditions [5].

Most work in this area has so far centered on finding the required control for a given $c(t)$. We have extended this idea to trajectory optimization. In a standard IDP, the original nonlinear system needs to be transformed into a system linearly dependent on the control vector [6]. This transformation facilitates a general methodology to solve for **u**. But for the current problem, our following treatment is more advantageous. To apply the idea of inverse dynamics more effectively, we first change the independent variable from t to θ. The system equations (1)–(5) with $\varepsilon = 0$ now become

$$\frac{dr}{d\theta} = r \tan\gamma \qquad (15)$$

$$\frac{dt}{d\theta} = \frac{r}{v \cos\gamma} \qquad (16)$$

$$\frac{dv}{d\theta} = \left(\frac{T \cos\alpha - D}{m} - \frac{\mu \sin\gamma}{r^2}\right)\frac{r}{v \cos\gamma} \qquad (17)$$

$$\frac{d\gamma}{d\theta} = \left(\frac{T \sin\alpha + L}{mv} + \left(\frac{v}{r} - \frac{\mu}{vr^2}\right)\cos\gamma\right)\frac{r}{v \cos\gamma} \qquad (18)$$

$$\frac{dm}{d\theta} = -\frac{T}{g_0 I_{sp}}\frac{r}{v \cos\gamma} \qquad (19)$$

Analogous to (13), we define

$$g = r(\theta) - c(\theta) = 0 \qquad (20)$$

In (20) $c(\theta)$ is a sufficiently smooth function which represents a specified altitude history. Differentiating (22) once with respect to θ gives

$$\tan\gamma = \frac{c'}{r} \qquad (21)$$

Differentiating (21) once again,

$$L(\alpha) = mv\left[(c'' - r\tan^2\gamma)\frac{v \cos^3\gamma}{r^2} - \left(\frac{v}{r} - \frac{\mu}{vr^2}\right)\cos\gamma - \frac{T \sin\alpha}{mv}\right] \qquad (22)$$

6

The prime in (21) and (22) stands for differentiation with respect to θ. Equations (21) determines the required γ for r to follow $c(\theta)$. Equation (22) provides the necessary lift control. For a specified thrust level T and current values of the state variables, Equation (22) constitutes an algebraic equation for α. With α solved from (22), Equations (17) and (19) can be integrated for v and m at next instant. So the solution of the system as well as the value of the performance index (fuel consumption, for instance) is completely determined by the choice of the pair of command altitude c and fuel-equivalence ratio ϕ. If we choose to represent $c(\theta)$ and $\phi(\theta)$ by certain smooth parametrized functions, the optimization problem reduces to a parameter optimization problem in which the best c and ϕ histories are iteratively sought through solving a sequence of inverse dynamic problems. Note that in the parametrization of c, one can always choose the boundary conditions

$$c(\theta_f) = r_0 + h_c \tag{23}$$

$$c'(\theta_f) = 0 \tag{24}$$

Then the first two of the three terminal constraints in (7) are automatically satisfied according to (20) and (21), leaving only the constraint on v_f to be met. With C_L represented by (6), α can be solved from (22) very effectively by Newton iterations with an accuracy of 10^{-6} frequently after only one iteration. Thus the computation of α does not pose extra burden since r and γ equations do not need to be integrated as a result.

With this inverse dynamics approach the trajectory is under more direct control of the parametrization process. Consequently, the sensitivity of the optimization problem is greatly reduced. In fact, with minimum efforts, one can easily construct various feasible trajectories that satisfy the terminal conditions (7) and state constraints (8) and (9) by choosing $c(\theta)$ and $\phi(\theta)$. This feature is not only essential to the success of the trajectory optimization, but may also be useful for quick design of hypersonic cruising trajectories (not necessarily optimal in any sense). Compared to the collocation method in Ref. [7], the current approach retains the merits such as better conditioning of the problem and robustness of the algorithm, while it cuts down the dimension of parametrization considerably for an accurate solution. Fewer optimization parameters directly contribute to a faster convergence. In addition, the inverse dynamics approach permits guidance commands to respond adaptively to perturbations, which will be discussed in later sections.

4. OPTIMAL SOLUTIONS

In order to gather sufficient information on the optimal trajectories, extensive runs have been performed to generate fuel-optimal trajectories. First, only constraint (8) is considered. The constraint (8) is handled by introducing a new state w_q

$$w_q(0) = 0, \quad \dot{w}_q = \begin{cases} -(q - q_{max}), & q > q_{max}; \\ 0, & q \leq q_{max}. \end{cases} \tag{25}$$

Constraint (8) is then equivalent to the terminal constraint

$$w_q(\theta_f) \geq 0 \tag{26}$$

A similar transform can be done for constraint (9). A squential quadratic programming algorithm [8] was used to solve the resulting constrained nonlinear programming problem. A parametric study on q_{max} was conducted. Figure 2 depicts variations of q for different values of q_{max}. In Fig. 3 are fuel-equivalence ratios for three trajectories. Figures 4 and 5 contain typical flight path angle and angle of attack histories and ascent altitude history. The wiggles on the q-histories in Fig. 2 are more likely a result of the finite-dimension approximation of the original optimal control problem than anything physically significant. The final masses for the optimal trajectories corresponding to different constraint levels are listed in Table 1.

Table 1. Summary of Optimal Solutions

$q \leq q_{max}$

q_{max} (psf)	∞	5000	4000	3000	2000
$m(t_f)$ (kg)	69859	68781	68525	68101	66351

General features of the optimal trajectories include:

(1) The trajectory typically divides into three stages: a quick climb out following takeoff, featuring large flight path angle and angle of attack; a relatively long mid-course cruise with small flight path angle and angle of attack, during which the constraint (8) is active; a final zoom into orbit.

(2) The optimal fuel-equivalence ratio stays almost unity during the midcourse cruise. Some modulation may be needed in the initial climb out to avoid violation of the constraint (8).

8

(3) When $q_{max} > 2500$ psf, the penalty of the constraint (8) on the fuel consumption is not very significant. The optimal trajectory simply takes longer flight time along the boundary $q = q_{max}$ to accelerate to the required orbital velocity. When q_{max} is below 2500 psf, the drag loss during the long cruise becomes significant, resulting in considerable increase in fuel consumption.

The observation (3) above prompts the question of what is the smallest q_{max} below which the NASP cannot achieve the orbital velocity with all the fuel it carries. The performance index this time should be

$$J = \max_{t_0 \leq t \leq t_f} q(t)$$

The corresponding optimal control problem is the so called minimax problem. The following transform converts this nonclassical optimal control problem into a parameter optimization problem, hence the present approach is still applicable.

$$\min q_{max}$$

$$q \leq q_{max}$$

$$m(t_f) \geq m_{min}$$

subject to system equations (1)–(5) and boundary conditions (7), where m_{min} is the mass of the aerospace plane excluding fuel. For our model, $m_{min} = 63,503$ kg (140,000 bf). q_{max} now is treated as an optimization parameter. For injection into the same orbit, the minimum q_{max} turns out to be 1499 psf with all fuel consumed (70,306 kg). The variation of q in this case is also plotted in Fig. 2.
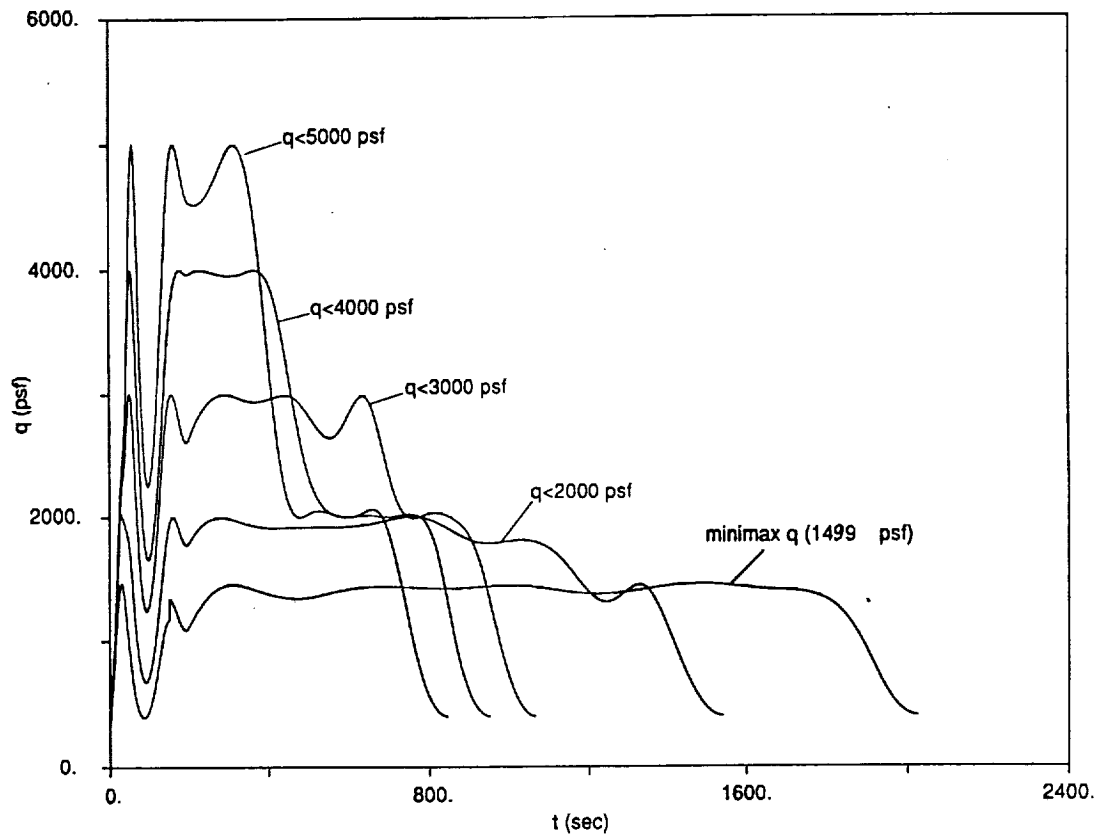
Figure 2. Variations of dynamic pressure q

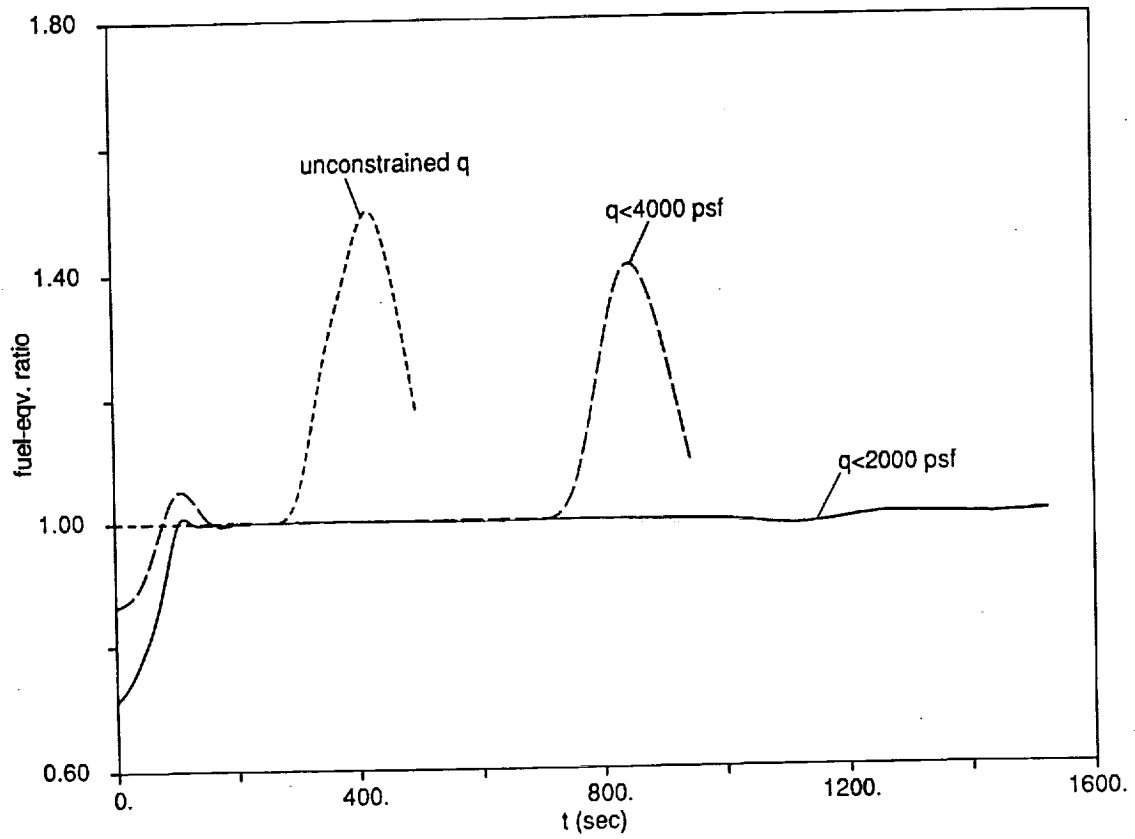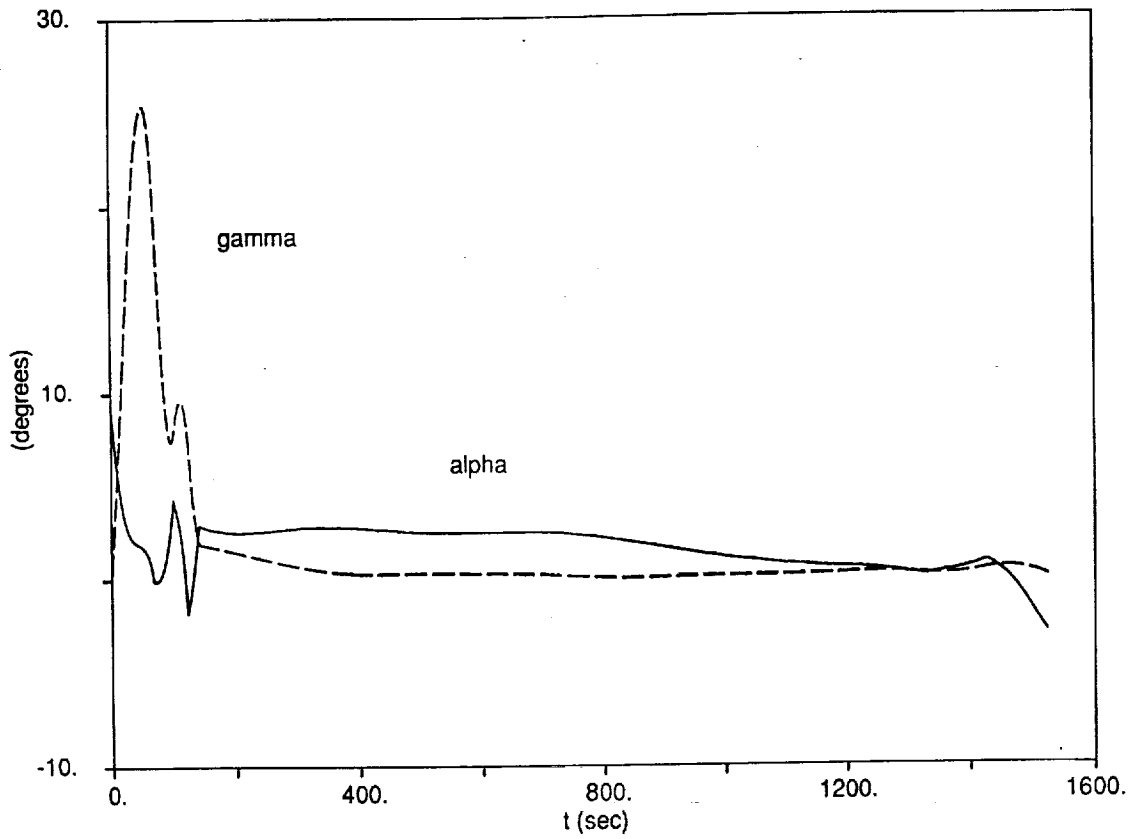10

Figure 3. Variations of fuel-equivalence ratio ϕ

Figure 4. Flight path angle γ and angle of attack α along the optimal trajectory $q \le 2000$ psf.
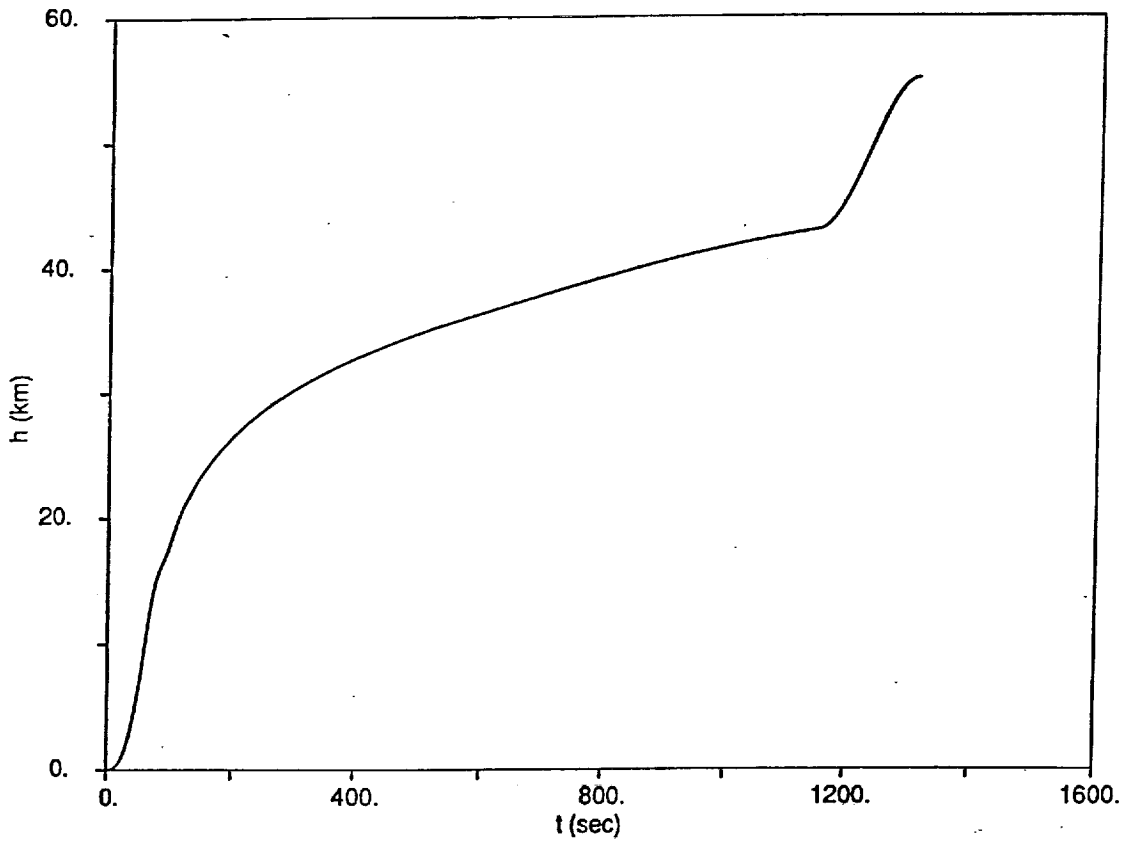
Figure 5. Optimal ascent altitude history ($q \leq 2000$ psf).

5. MIDCOURSE FEEDBACK CONTROLLER AND SIMPLIFIED SOLUTIONS

As we have observed, the prominent features of the midcourse include slowly-varying γ, small α, fuel equivalence ratio of nearly unity, and observance of $q = q_{max}$. On the basis of these observations, we can develop a nonlinear feedback midcourse controller that maintains these features of the trajectory.

We set $\phi \equiv 1$ after initial climb out. Since $\dot{\gamma} \approx 0$ and α is small in the midcourse, letting $\dot{\gamma} = 0$ and neglecting $T \sin \alpha$ in Eq. (4) lead to

$$L = m(\frac{\mu}{r^2} - \frac{v^2}{r}) \cos \gamma \tag{27}$$

(27) is essentially the same as the reduced solution in Re.f [4] in which it is derived based on a singular perturbation method. In light of our optimal solution, the validity of the time scale decomposition is confirmed for the midcourse. Nonetheless, (27) is not a valid approximation for the initial climb during which both $\dot{\gamma}$ and γ have large values.

Controller (27) does not have the mechanism to enforce state inequality constraints. However, we have observed that the optimal trajectory climbs on boundary $q = q_{max}$ and $Q = Q_{max}$ in sequence during the midcourse. To renforce the constraints on the basis of (27), a midcourse feedback controller

$$\alpha = \begin{cases} m(\mu/r^2 - v^2/r)\frac{\cos \gamma}{qS_{ref}C_{L1}} + k_1(q - q_{max}) + k_2\dot{q}, & \text{if } Q < Q_{max} \\ m(\mu/r^2 - v^2/r)\frac{\cos \gamma}{qS_{ref}C_{L1}} + k_3(Q - Q_{max}) + k_4\dot{Q}, & \text{if } Q \geq Q_{max} \end{cases} \tag{28}$$

is proposed. The feedback gains k_i's are properly chosen constants. In fact, controller (28) can be used to track any hypersurface $F - F_{ref} = 0$ when F is a given function of the altitude and some other state variables. If F is a monotonic function of the altitude, which is the case for q and Q, constant coefficients k_i's will suffice.

With the aid of controller (28), the simplified trajectory is planned in the following sequence: For the initial climb $\theta \in [0, \theta_1)$, both $\phi(\theta)$ and $c(\theta)$ are parametrized by cubic splines as before. For the midcourse $\theta \in [\theta_1, \theta_2)$, let $\phi = 1$, and α be given by (28). The final zoom part $\theta \in [\theta_2, \theta_f]$ is characterized by letting $\phi = 1$ and

$$c(\theta) = a + b\theta + d\theta^2 + e\theta^3 \tag{29}$$

Equation (29) determines the angle of attack control for the final zoom via the inverse dynamics. θ_1, θ_2, θ_f, $c(\theta)$ and $\phi(\theta)$, $\theta \in [0, \theta_1]$, are to be optimized. The coefficients in

14

(29) are determined by the continuity conditions $c(\theta_2) = r(\theta_2)$, $c'(\theta_2) = r(\theta_2)\tan\theta_2$, and the terminal conditions (23) and (24).

Planned in such way, the dimension of the optimization parameter vector is reduced almost by two thirds, down from over 30 to 12, which contributes to a much faster convergence of the optimization process. More significantly, the conditioning of the problem is further improved to such an extent that the rather difficult original optimization problem now becomes an easy routine operation. The fuel consumption is further reduced because the midcourse controller tracks the boundary $q = q_{max}$ better than the control α obtained through finite-dimension parametrization, hence the efficiency of the the air-breathing engine is better. For instance, the constrained solution with $q \leq 95,760$ N/m² yields a final mass of 67,112 kg, greater than the previously obtained value of 66,351 kg in Table 1. Figure 6 shows the q-history and Q-history along the optimal trajectory under the controller (28) with $q \leq 95,760$ N/m² and $Q \leq 800$ Watt/cm², where the heating rate Q is modeled by

$$Q = (4.919 \times 10^{-8})\rho^{0.5}v^{3.0} \qquad (30)$$

In (30) density ρ is in kg/m³ and velocity v is in m/sec, and (30) corresponds to equilibrium conditions on the surface of a wing leading edge 10 cm in radius [4]. Shown in Fig. 7 is the ascent altitude history for the same trajectory.

In closing this section, we conclude that control law (28) not only greatly improves the process of off-line generation of the optimal solution, but is also particularly attractive for real-time onboard applications, because the controller demands no intensive calculations for implementation. The simplified optimal solution provides an fairly efficient and reliable way of investigating the optimal trajectories of a very difficult problem. Because of the feedback nature of the midcourse controller, even under the off-nominal flight conditions the controller is still able to prevent sizable violation of constraints (8) and (9).

2400.

1600.

q(psf), Q(Watt/cm**2)

800.

0.

q
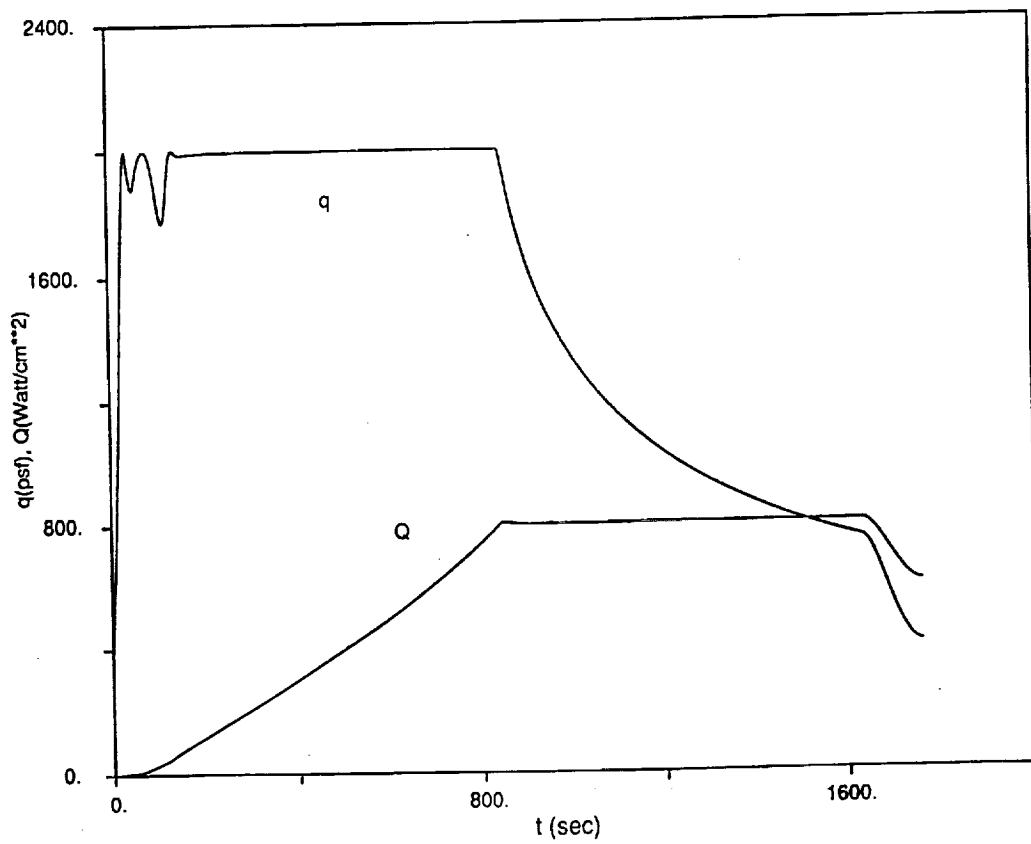
Q

0.   800.   1600.

t (sec)

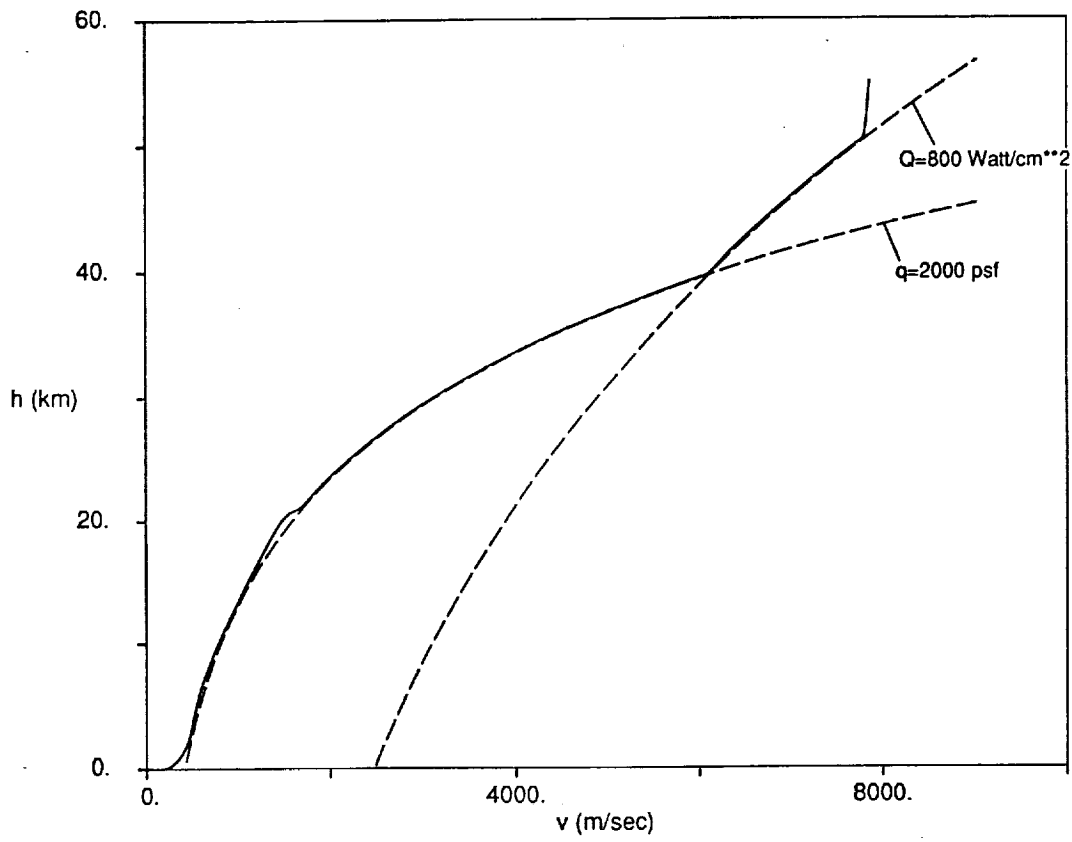**Figure 6.** Variations of dynamic pressure ($q \leq 2000$ psf) and heating rate ($Q \leq 800$ W/cm^2).

Figure 7. Optimal ascent altitude history ($q \leq 2000$ psf, and $Q \leq 800$ W/cm^2).

6. ASCENT GUIDANCE

In addition to the ever exsiting environmental disturbances, the unprecedented nature of the NASP increases the likelihood of system uncertaintities and modeling inaccuracy. All these factors make it imperative that the NASP have a robust guidance system that can direct the vehicle to fulfil its mission in the presence of the disturbances and perturbations. The inverse dynamics approach introduced in Section 3 renders a powerful tool in this regard.

Once a nominal optimal trajectory for a flight vehicle is designed, there are two types of popular guidance strategies. In the first strategy corrective actions based on deviations of the actual trajectory from the nominal are taken to restore the flight path. The second strategy recalculates a new trajectory on-line based on current state if deviations occur, using techniques such as neighbouring extremal control and singular perturbations. As we shall see, the inverse dynamics approach in conjunction with appropriate feedback compensation offers a blend of the above two strategies, and appears to offer both robustness and suitability for real-time environment

Suppose that the equivalence ratio ϕ^* and command altitude c^* have been obtained off-line for an optimal ascent trajectory of the NASP. The generation of the corresponding angle of attack command $\tilde{\alpha}$ from

$$L(\tilde{\alpha}) = mv[(c^{*\prime\prime} - r\tan^2\gamma)\frac{v\cos^3\gamma}{r^2} - (\frac{v}{r} - \frac{\mu}{vr^2})\cos\gamma - \frac{T\sin\tilde{\alpha}}{mv}] \qquad (31)$$

only requires minimum computation and should be easily carried out onboard. The values of the state variables in (31) are the actual values instead of nominal ones. $\tilde{\alpha}$ so generated is adaptive to perturbations and disturbances when they are known. The idea is equivalent to solving the inverse dynamic problem for a different system to generate the same output. For instance, if the atmospheric density has fluctuations, as it always will happen, and they are measured instantly, the terms involving ρ in Eq. (31) can be assigned the correct value. $\tilde{\alpha}$ so computed would result in $d\gamma/d\theta = d\gamma^*/d\theta$, then $\gamma(\theta) = \gamma^*(\theta)$ and $r(\theta) = r^*(\theta)$ if there are no initial errors, where the quantities with asterisk are the nominal values. Nonetheless, perturbations and disturbances are not always known to the onboard computer. Additional feedback terms may be added to compensate the inaccuracy in more general situations. A such candidate is

$$\alpha = \tilde{\alpha} - k_h(h - h^*) \qquad (32)$$

18

where $k_h \geq 0$ is guidance constant. When perturbations and/or disturbances are known, α reduces to $\tilde{\alpha}$ since $h = h^*$. The deviations in velocity are very effectively compensated by fuel-equivalence ratio

$$\phi = \phi^* - k_v(v - v^*), \quad k_v > 0 \tag{33}$$

To test the effectiveness of (32) and (33), the simplified fuel-optimal trajectory with $q \leq 95,760$ N/m^2 is chosen to be the nominal. Equations (32) and (33) are applied in the initial climb and final zoom. The midcourse is still controlled by (28) without modification, which assures that no excessive violation of the state constraints would occur along the perturbed trajectories. Some typical sources of errors are examined in the following.

Density Fluctuations

Assume that the actual atmospheric density is varying according to

$$\rho = (1 + 0.2\sin\frac{2\pi h}{50})\rho^* \tag{34}$$

In (34) ρ^* is the nominal density. h is altitude in km. The maximum fluctuation of 20% as given by (34) is a modest variation of the density compared with the flight data of the Space Shuttle [9].

(a) The variation is measured and known to the onboard computer. By the above arguements, h and γ will follow their nominal histories exactly. With (33) the final error in velocity was only $\Delta v_f = 0.97$ m/sec.

(b) Suppose that the density variation is not known to the onboard computer. Figure 8 exhibits the comparison of the nominal trajectory with two perturbed trajectories: (1) Perturbed trajectory I used the nominal density to calculate $\tilde{\alpha}$ and the controls were obtained from (32) and (33). Final orbital insertion errors were $\Delta v_f = -1.66$ m/sec, $\Delta h_f = 0.747$ km and $\Delta \gamma_f = 0.37°$. (2) Perturbed trajectory II was flown with the preprogrammed nominal optimal α^* and ϕ^*. The open-loop controls resulted in a crash.

Lift Coefficient Variation

Suppose that a uniform inaccuracy in C_L exists such that C_L only has 90% of its nominal value

$$C_L = 0.9C_L^* \tag{35}$$

19

(a) If the inaccuracy can be identified in flight, $\tilde{\alpha}$ can be calculated using the true values of C_L. The only terminal error was in v which was reduced to $\Delta v_f = -0.72$ m/sec by (33).

(b) More likely the true values of C_L will not be exactly known. $\tilde{\alpha}$ will be computed with the nominal value C_L^*. Two perturbed trajectories, again denoted as perturbed I and II as in above, are plotted in Fig. 9. Trajectory perturbed I which was controlled by (32) and (33) nearly followed the nominal. The difference is virtually disernible to the scale of the plot. Final errors were $\Delta v_f = -0.99$ m/sec, $\Delta h_f = 0.17$ km and $\Delta \gamma_f = 0.021°$. The open-loop nominal controls failed to steer perturbed II to achieve the final orbit. In fact, the two dives along trajectory perturbed II generated huge peak dynamic pressure ($>$2,000,000 N/m^2) that would have already crushed the vehicle.

Thrust Inaccuracy

Another source of perturbations is the model inaccuracy of the airbreathing propulsion system. Suppose that a 5% loss in actual thrust level attributed to the model inaccuracy exists:

$$T = 0.95T^* \tag{36}$$

The largest error in this case will be in velocity, since the flight path is mostly controlled by the angle of attack. The simple compensation (40) helps reduce the velocity error remarkably, resulting in $\Delta v_f = -0.73$ m/sec while $\Delta v_f = -158.3$ m/sec without compensation in ϕ.
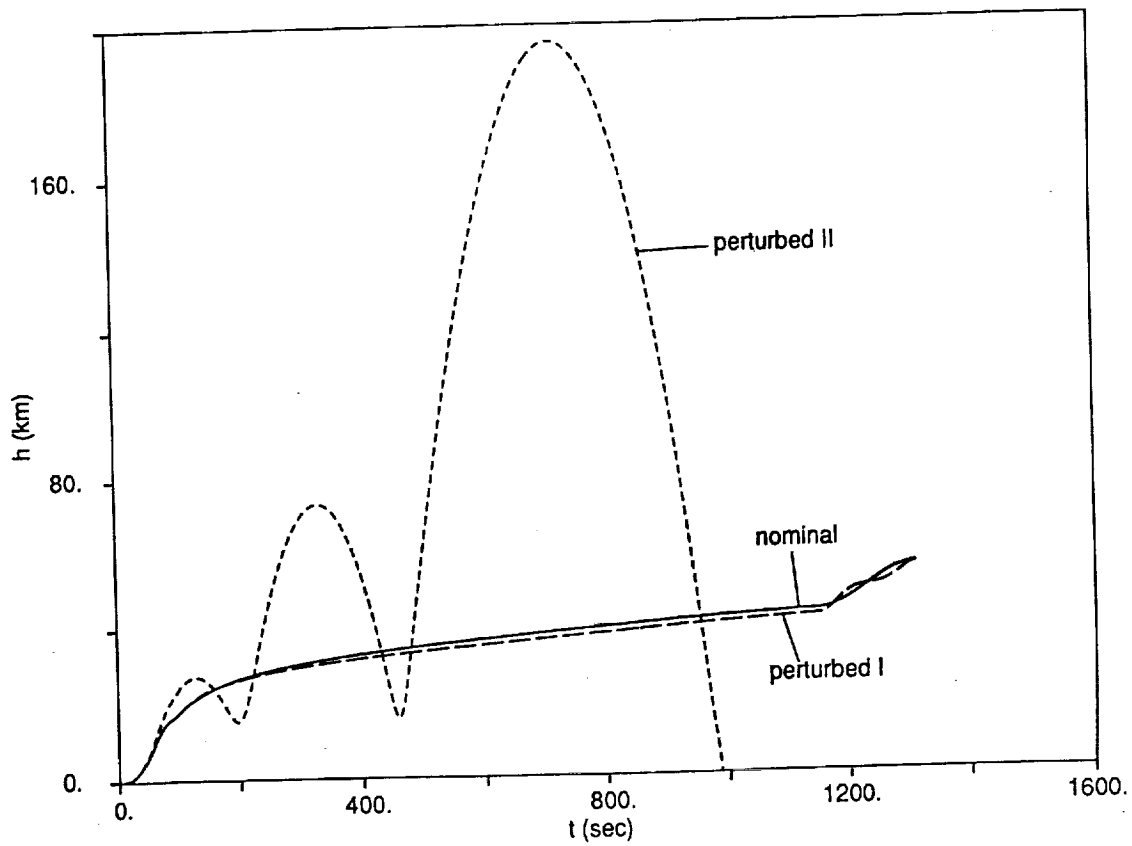
20

Figure 8. Comparison of trajectories in the presence of atmospheric density fluctuation: nominal=optimal trajectory ($q \leq 2000$ psf); perturbed I=trajectory flown with guidance laws (27), (28) and midcourse controller (26); perturbed II=trajectory flown with preprogrammed nominal controls

Figure 9. Comparison of trajectories in the presence of lift modeling inaccuracy: nominal=optimal trajectory ($q \leq 2000$ psf); perturbed I=trajectory flown with guidance laws (27), (28) and midcourse controller (26); perturbed II=trajectory flown with preprogrammed nominal controls
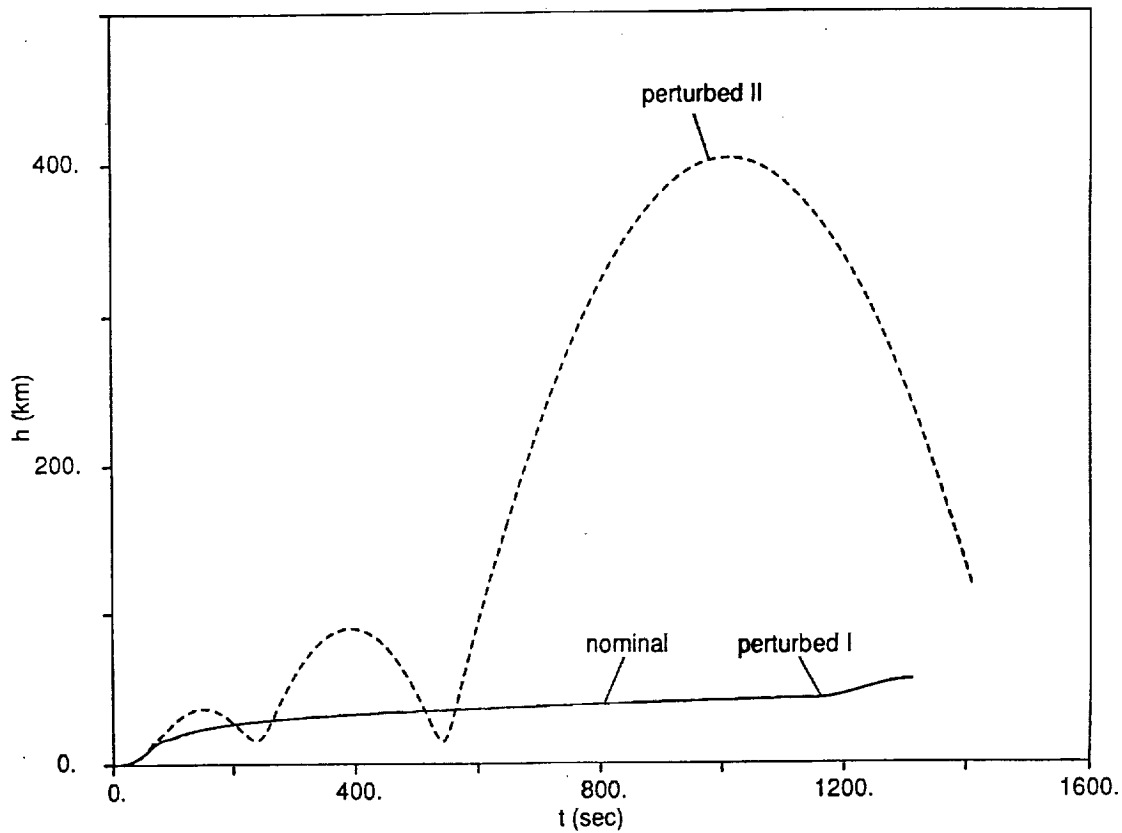
22

7. ROCKET-ASSISTED ASCENT

7.1 Singular Control Analysis

When the orbital altitude is higher, during the final push the airbreathing propulsion system, supersonic ramjets (SCRAM jets), may become ineffective as the atmosphere gets thinner. A rocket will be needed. Calise *et al* show that the SCRAM jets may still stay on for the remaining flight even if they are not effective [10]. Practically, the SCRAM jets may be cut off at an optimal point. Assuming a throttable rocket, the remaining rocket-assisted trajectory could consist of a combination of coasting, singular thrust and full-throttle arcs. We shall examine the possibility of singular arc first. Let $\alpha = 0$ after the SCRAM jets are turned off. By the standard optimal control theory [11] and system (1)–(5), we have the Hamiltonian

$$H = p_r v \sin\gamma + p_v \frac{T\cos\varepsilon}{m} - p_v(\frac{D}{m} + \frac{\sin\gamma}{r^2}) - p_\gamma \frac{T\sin\varepsilon}{mv} + p_\gamma(\frac{v}{r} - \frac{\mu}{vr^2})\cos\gamma - p_m \frac{T}{g_0 I_{sp}} = 0 \tag{37}$$

The switching function is

$$S = vp_v \cos\varepsilon - p_\gamma \sin\varepsilon - \frac{mvp_m}{g_0 I_{sp}} \tag{38}$$

where for the rocket, I_{sp} is considered constant. The optimal thrust is given by

$$T^* = \begin{cases} 0, & S < 0; \\ 0 < T^* < T_{max}, & S \equiv 0; \\ T_{max}, & S > 0. \end{cases} \tag{39}$$

The first case in (39) corresponds to a coasting arc, second to a singular arc. The optimal thrust angle is derived from $\partial H/\partial\varepsilon = 0$:

$$\tan\varepsilon^* = -\frac{p_\gamma}{vp_v} \tag{40}$$

By the minimum principle [10], the matrix

$$\mathbf{H}_{uu} = \begin{pmatrix} \partial^2 H/\partial\varepsilon^2 & \partial^2 H/\partial\varepsilon\partial T \\ \partial^2 H/\partial T\partial\varepsilon & \partial^2 H/\partial T^2 \end{pmatrix} \tag{41}$$

must be positive semidefinite along an optimal solution. It is obvious by (37) and (40) that $\partial^2 H/\partial T^2 = 0$ and $\partial^2 H/\partial\varepsilon\partial T = \partial^2 H/\partial T\partial\varepsilon = 0$. On singular arc one can show by using $S = 0$ that

$$\frac{\partial^2 H}{\partial\varepsilon^2} = -\frac{mp_m v}{g_0 I_{sp}} \tag{42}$$

23

Since p_m represents the sensitivity of the minimization performance index $J = -m(t_f)$ with respect to variation of m, p_m should always be negative. In fact, if drag $D = 0$, one can arrive at, with the aid of adjoint equations $\dot{\mathbf{p}} = -\partial H/\partial \mathbf{x}$ and transversality conditions, the relationship

$$p_m(t) = -\frac{m(t_f)}{m(t)} \tag{43}$$

In conclusion, we see that $\partial^2 H/\partial \varepsilon^2 > 0$, or equivalently, $\mathbf{H}_{uu}$ is positive semi-definite. The necessary conditions for optimality do not exclude the possibility of singular arc. Other tests for the optimality of singular control (e.g. Ref. [12]) are difficult to apply here due to the complexity of the system. But given the observation that at higher altitudes where aerodynamic drag is small, a sustained thrusting arc can be beneficial to the buildup of the insertion velocity, singular arc may exist. However, analysis in the Appendix asserts that *if the final orbit is circular, the optimal arc immediately before orbital insertion must be a full-throttle one.*

On singular arc, it is shown in the Appendix that $z = \tan(\varepsilon/2)$ satisfies

$$Az^4 + Bz^3 + Cz^2 + Ez + F = 0 \tag{44}$$

where A, B, C, E and F are functions of the state variables. In particular, if $|\varepsilon| << 1$, we have

$$\tan \frac{\varepsilon}{2} \approx -\frac{F}{E} = \frac{\sin\gamma[Dr^2(v + g_0 I_{sp}) - m\mu g_0 I_{sp} \sin\gamma]}{2(m\mu g_0 I_{sp} \sin 2\gamma + r^2 v D \cos\gamma)} \tag{45}$$

The throttle on a singular arc can in principle be obtained in a similar way, only the expression turns out to be excessively complicated.

Within the framework of nonlinear programming approach, the possibility of coasting and singular thrust arcs is conveniently handled. The complete ascent trajectory with rocket assistance is parametrized in the following sequence: airbreathing-engine powered ascent portion as before; a coasting arc following the cutoff of the SCRAM jets with $\alpha = 0$; rocket-assisted flight to orbital insertion. The optimization parameters include all those used in previous sections plus time durations of coasting and rocket-assisted flight, as well as those that specify the rocket throttle and ε programs.

7.2 Feedback Control Laws via Inverse Dynamics

Despite that the analysis suggests possible combination of singular/full-throttle arcs, it was found that the fuel-consumption is not sensitive to the rocket throttle program at all. The reason is that after a long coast the rocket is turned on at approximately the

orbital altitude. The optimal $|\varepsilon|$ then is almost zero and the major role of the rocket is to push the velocity to orbital speed. Since drag D is very small at that altitude, the situation is similar to a rocket with fixed ε in vacuum–the velocity increament is only dependent on the rocket fuel expenditure, independent of the throttle program. Numerical results show that allowing throttle to vary between $[0, T_{max}]$ yields negligible improvement in the fuel-consumption (only few kilograms of fuel saving) as compared with the case of full-throttle. Nevertheless, using intermediate thrust level of a throttable rocket can be rather advantageous in achieving orbital insertion accurately. To show this, we again adopt the inverse dynamics approach. Let the command altitude $c(\theta)$ and a desired history of velocity $v(\theta)$ be specified for the rocket-assisted portion of the trajectory. In a similar way as Eq. (22) is derived, we have

$$T \sin \varepsilon = (\frac{v}{r} - \frac{\mu}{vr^2})mv \cos \gamma - \frac{mv^2 \cos^3 \gamma}{r^2}(c'' - r \tan^2 \gamma) \triangleq U \qquad (46)$$

$$T \cos \varepsilon = \frac{mv \cos \gamma}{r}v' + \frac{\mu \sin \gamma}{r^2} + D \triangleq V \qquad (47)$$

Two resulting feedback control laws are

$$\eta = \frac{1}{T_{max}} \sqrt{U^2 + V^2} \qquad (48)$$

$$\tan \varepsilon = \frac{U}{V} \qquad (49)$$

where η represents the throttle of the rocket, and T_{max} the maximum available thrust. Instead of optimizing $c(\theta)$ and $v(\theta)$, we find it sufficient to let

$$c(\theta) = a + b\theta + d\theta^2 + e\theta^3 \qquad (50)$$

$$v(\theta) = n + p\theta \qquad (51)$$

With the rocket thrusting duration being an optimization parameter, the coefficients a, b, d and e in (50) are determined by the continuities of r and γ at the instant θ_r when the rocket is turned on, and by Eqs. (23) and (24) for the first two terminal constraints in Eqs. (7). Coefficients n and p are defined by the continuity of v at θ_r and the final constraint in (7). Since these calculations can be easily done onboard, the near-optimal parametrizations (50) and (51) have a distinct advantage: the orbital insertion conditions (7) will remain satisfied even if the actual trajectory deviates from the nominal at θ_r. This is because (50) and (51) always lead the trajectory from the states at θ_r, whatever

the values are, to the target point defined by Eqs. (7) when the coefficients are calculated with the actual values of the states at θ_r. The corresponding inverse controls (48) and (49) are hence disturbance-accommodating, provided that they are not in violation of the control constraints $|\varepsilon| \leq \varepsilon_{max}$ and $\eta \leq 1$.

A typical near-optimal rocket-assisted trajectory for circular orbital insertion at $h_f = 92.6$ km (50 nm) subject to constraints (8) and (9) is plotted in Fig. 10. The points of interest are marked. In particular, the SCRAM jets are found to be turned off at 70 km. Following a coast of 452 seconds, a throttable rocket with $T_{max} = 266,893$ N (60,000 lb) and $I_{sp} = 440$ seconds starts firing at 92.3 km with an intermediate throttle of about 0.21. Orbital insertion is achevied 88.5 seconds after the rocket ignition. The final mass is 64,931 kg, which is comparable to $m_f = 65,370$ previously obtained for $h_f = 55$ km without rocket-assistance. It should be noted that the coasting arc saves fuel significantly (more than 3,000 kg) by allowing at no cost the change of kinetic energy generated by the airbreathing propulsion to potential energy at higher altitude.

7.3 Guaranteed Orbital Insertion

The guarantee of accurate orbital insertion with the inverse control of the rocket in the presence of disturbaces and perturbations is demonstrated by introducing atmospheric density fluctuations. Vertical variation (34) and the following longitudinal variation

$$\rho = (1 + 0.2 \sin \frac{2\pi d}{1000})\rho^* \tag{52}$$

are used, where in (52) $d = r_0\theta$ (km) is the down range. Assuming that the actual ρ is not known to the onboard computer, the airbreathing propulsion portion of the trajectory is controlled by the midcourse controller (28) and the guidance laws (32) and (33). These measures have already greatly reduced the deviations of the perturbed trajectories, which prevents the trajectories from entering unrecoverable regions of the rocket. Then after the coast the inverse rocket control laws (48) and (49) adaptively steer the aerospace plane to an accurate orbital insertion. Figure 11 contains the nominal and the two perturbed trajectories. The final masses of the perturbed trajectories are 64,635 kg and 64,202 kg, respectively. The longitudinal ρ fluctuation is more harmful to trajectory control than the vertical deviation. This is no supprise if one compares the down range the aerospace plane travels (about 14,300 km) with the altitude gained (92.6 km). The oscillations of altitude along the perturbed trajectory II in Fig. 11 suggest that the midcourse controller (28) is at work, tracking the q and Q-constraints accurately even in the presence of the

26

sinusoidal perturbation of the atmospheric density. The variation of the corresponding α is shown in Fig. 12. Figure 13 depicts the histories of q and Q in this perturbed situation. The nominal and perturbed rocket throttle settings η and thrust angles ε are shown in Figs. 14 and 15. The effect of controls adapting to disturbances are clearly seen.
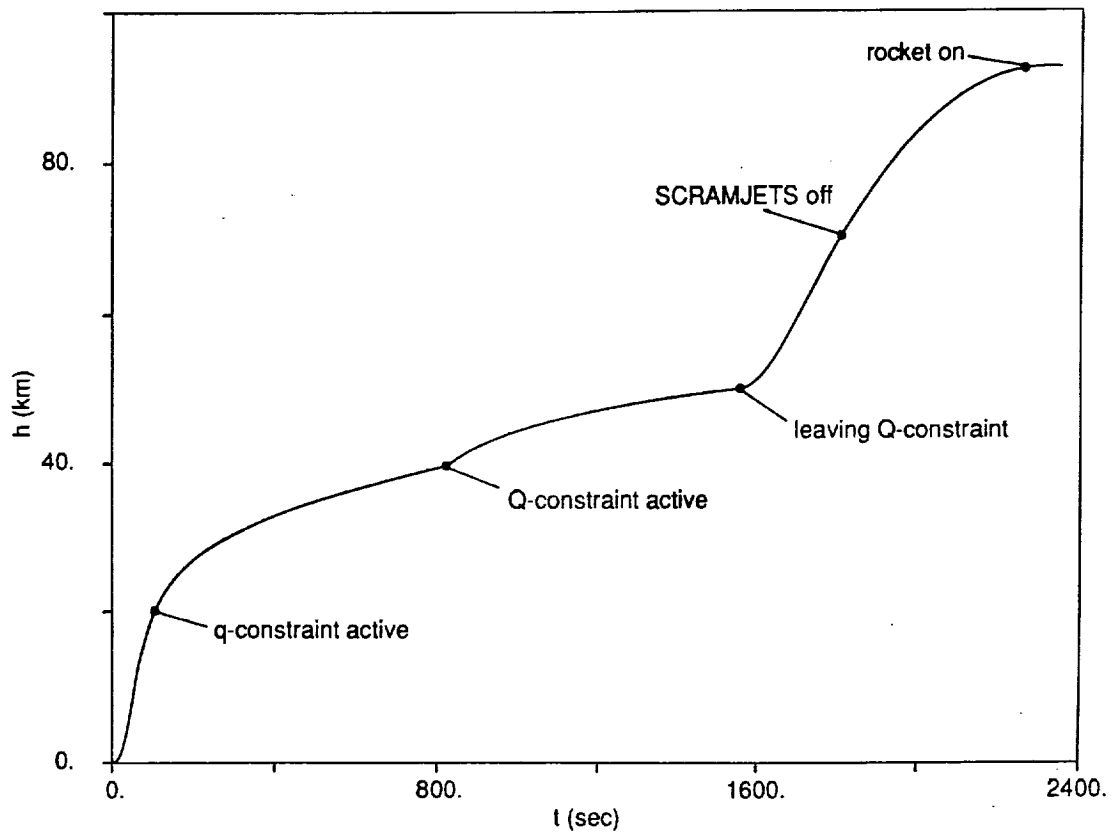
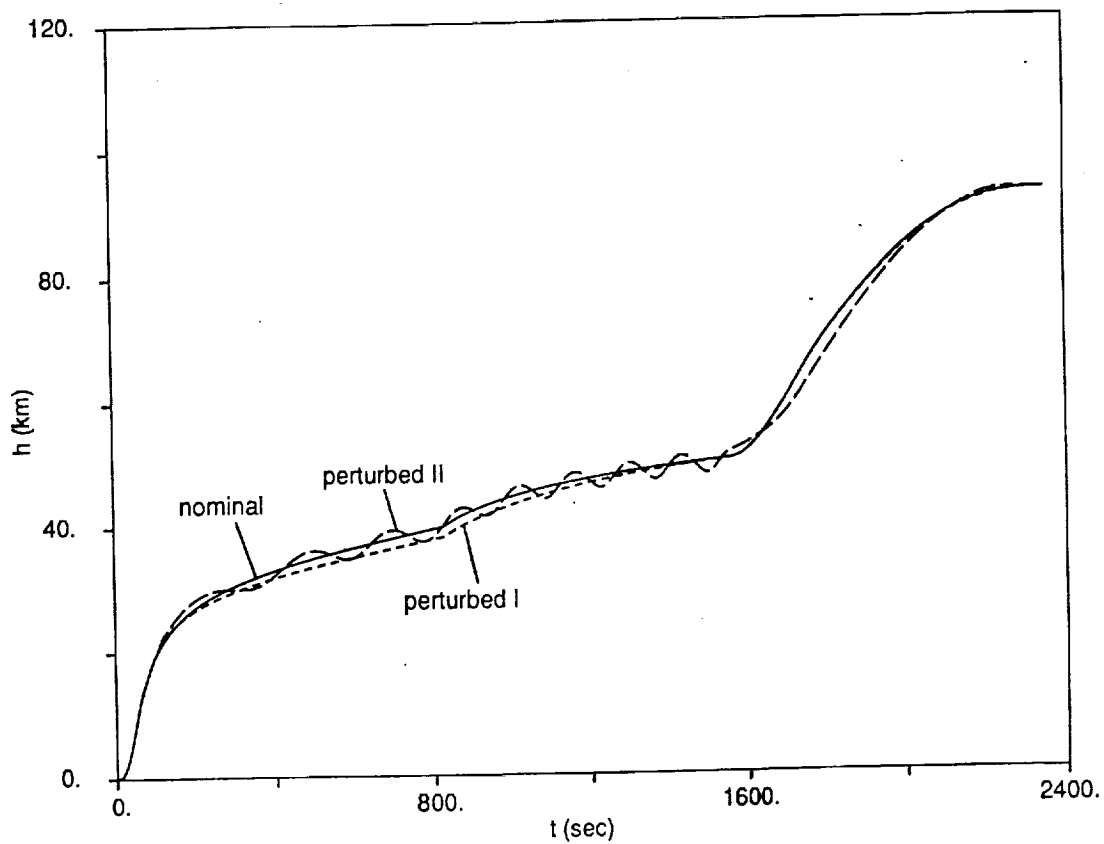**Figure 10.** Typical rocket-assisted optimal ascent

Figure 11. Comparison of rocket-assisted trajectories: nominal=optimal trajectory in Fig. 10; perturbed I= trajectory subject to vertical atomspheric density fluctations; perturbed II=trajectory subject to horizontal atomspheric density fluctations.
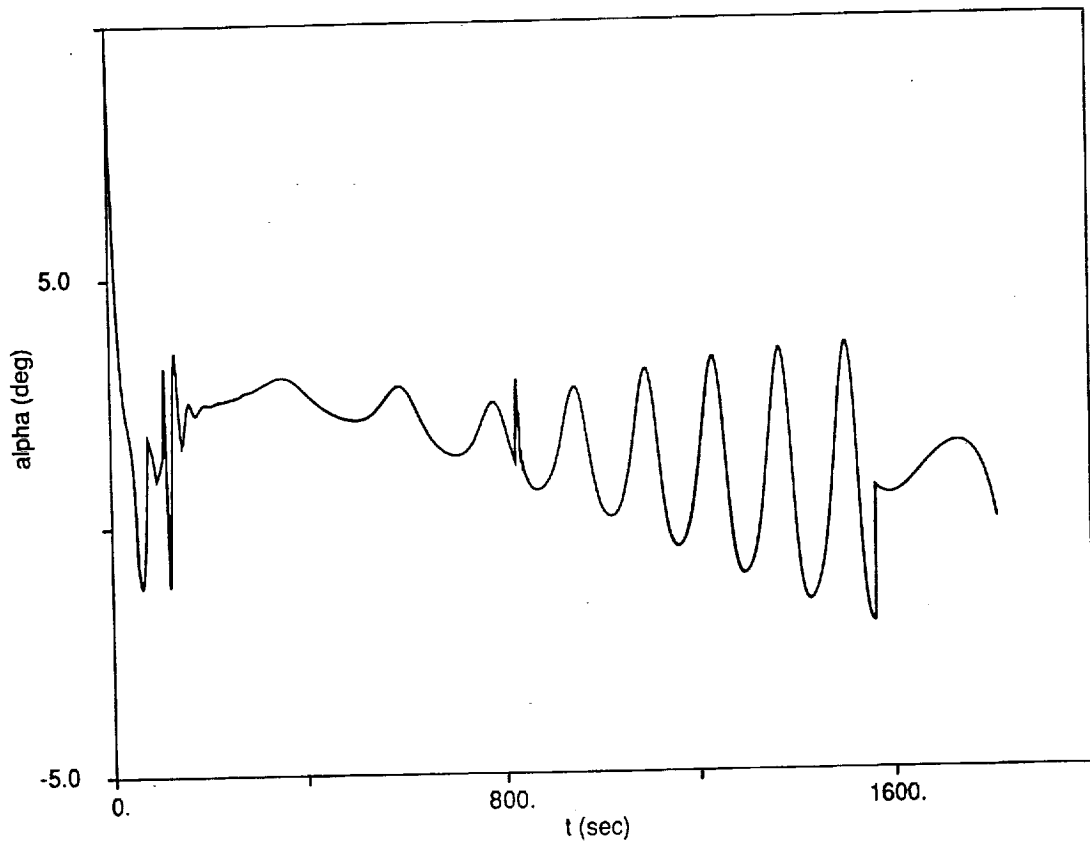
Figure 12. Variation of angle of attack along the trajectory (perturbed II) subject to horizontal sinusoidal atmospheric density fluctuations.
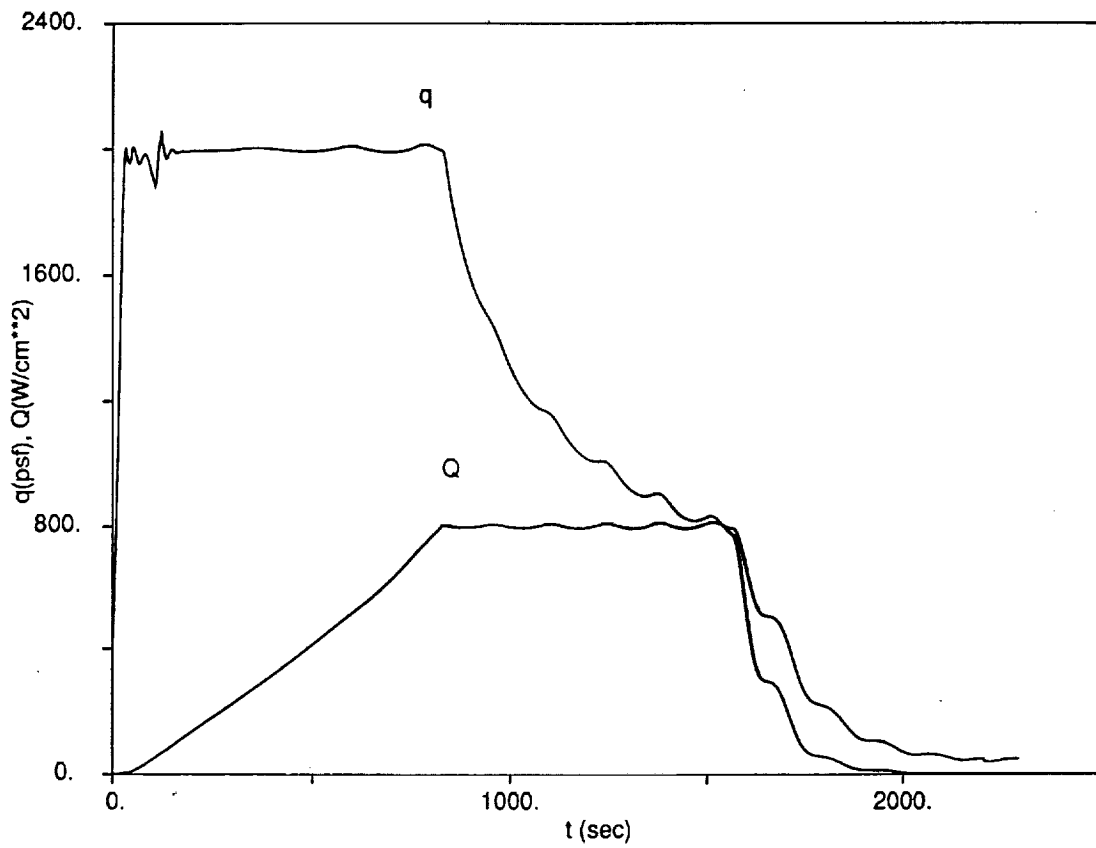
Figure 13. Variations of dynamic pressure q and heating rate Q along the trajectory (perturbed II) subject to horizontal sinusoidal atmospheric density fluctuations.
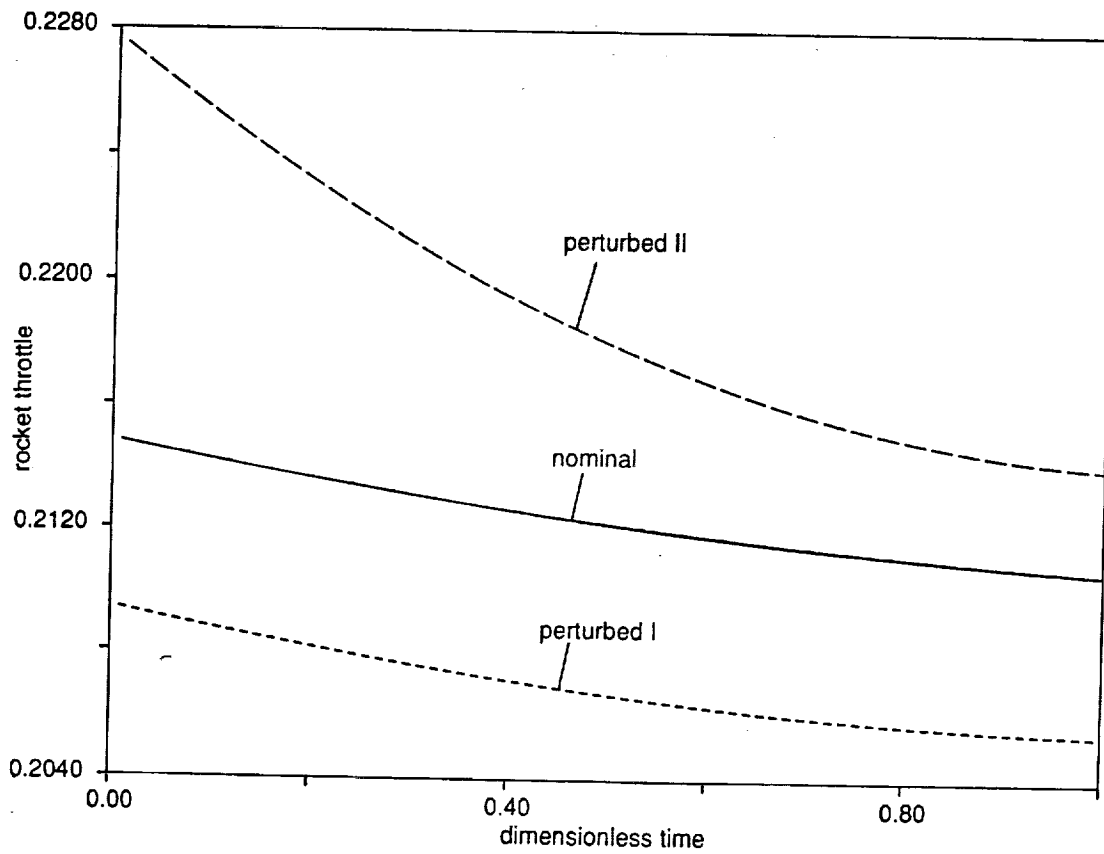
Figure 14. Comparison of rocket throttle settings along rocket-assisted trajectories (perturbed I and II are defined the same as in Fig. 11).
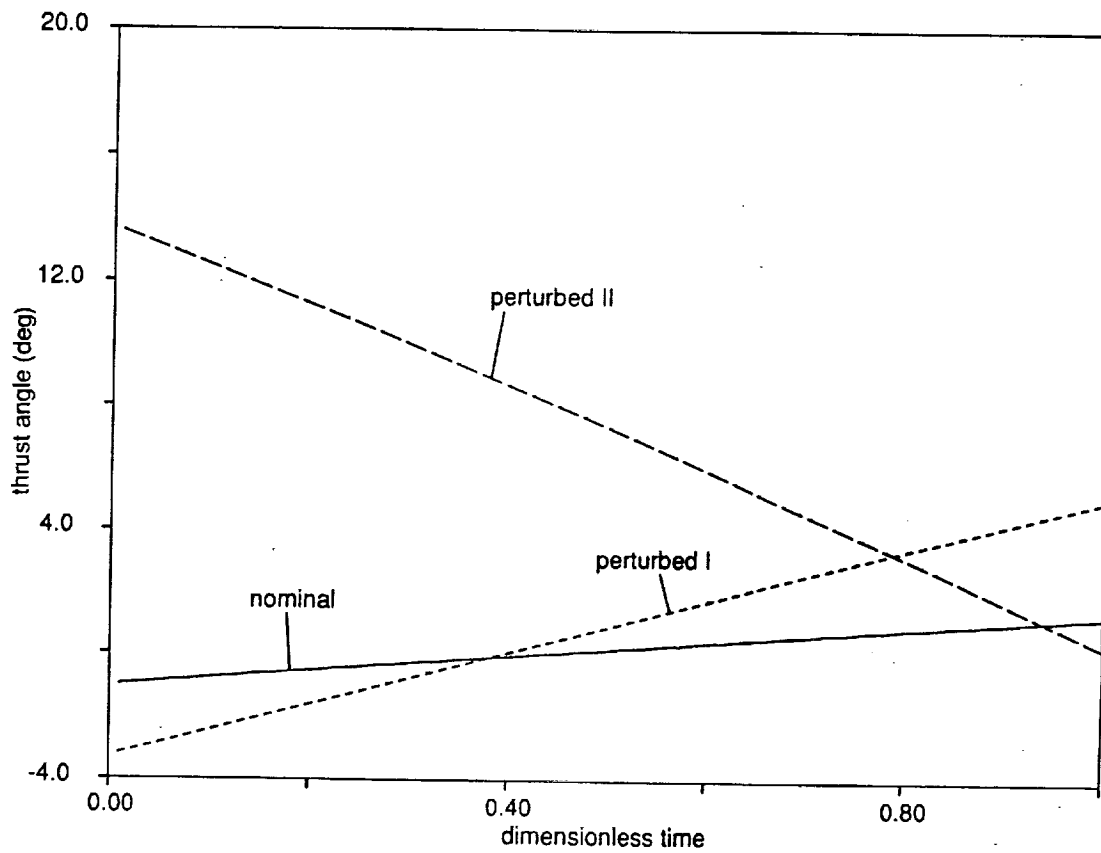
Figure 15. Comparison of rocket thrust angles along rocket-assisted trajectories (perturbed I and II are defined the same as in Fig. 11).

8. CONCLUSIONS AND FUTURE RESEARCH

The trajectory optimization problem for the National AeroSpace Plane has been formulated as an inverse dynamic optimization problem. Extensive numerical expreiments have been conducted. The approach has proven effective in solving this otherwise very difficult problem with relative ease. Generalization of similar approach to some other difficult optimization problems may be worthwhile. Both classical performance index – minimum-fuel and nonclassical performance index – minimax dynamic pressure are considered. The results lead to a better understanding of the characteristics of hypersonic flight. A nonlinear feedback midcourse controller suitable for onboard implementation is proposed, which also significantly further simplifies and improves the solution. Robust ascent guidance is obtained by using combination of feedback compensation and onboard generation of control through the inverse dynamics approach. Optimal rocket-assisted trajectories are investigated. The pattern of the optimal tajectory is found to be airbreather-powered ascent + coast + rocket-assist. The last arc immdediately before insertion onto a circular orbit must be a full-throttle arc. Inverse rocket control laws are developed that together with the ascent guidance scheme guarantee accurate orbital insertion even in the presence of disturbances and system uncertaintities. This work has also prompted the following thoughts that warrant further investigation:

1. Analysis of Constrained Trajectories

As found in above sections, the dominant portion of the optimal ascent trajectcory lies on the boundaries of the dynamic pressure and heating rate constraint. It is believed that accurate approximate analytical solution of time to the constrained portion of the trajectory is possible. An enlightening treatment for a special case is presented in Ref. [13] in which the constrained dynamic system is shown to be a two-time-scale system and asymptotic analytical solution is obtained. The idea begins with a careful examination of the constrained flight of an aerospace vehicle

$$\dot{\mathbf{x}}(t) = \mathbf{f}(x, u) \tag{53}$$

$$C(h, \rho(h), v) = 0 \tag{54}$$

where Eq. (53) is the state equation and $\mathbf{x}$ is the state vector which typically consists of h (altitude), θ (polar angle), γ (flight pathe angle), v (speed) and m (mass). $\mathbf{u}$ is the control. Equation (54) is a nonlinear algebraic flight path constraint. ρ in (2) represents the

atmospheric density. By properly choosing a set of nondimensional variables and studying the predominant factors of the constrained motion, it may be possible to reveal that a natural two-time-scale property exists so that the flight path angle dynamics can be considered "fast" as compared to the altitude dynamics. With the aid of singular perturbation theory, it may be possible to obtain approximate analytical asymptotic solutions of time. Then the trajectory optimization and guidance problem will be significantly simplified.

2. Application of Simulated Annealing Algorithm

While the inverse dynamics approach has been quite successful, it requires the problem to be sufficiently smooth. The smoothness is achieved by using analytical fitting to the key aerodynamic coefficients. This may or may not be done in a reasonably efficient way, depending on the problem. In our previous endeavors this was fortunately the case. If a complete model of the aerospace plane is totally based on linear interpolations of tabulated data, which is most likely for a realistic vehicle, the trajectory optimization problem is inherently nonsmooth, although continuous. The nonsmoothness can cause serious convergence problems if optimization algorithms based on gradients are used. A genetic algorithm, a nongradient type method, has been tested on a similar problem[5]. We will propose to use another type of nongradient method, continuous simulated annealing algoritm [14], on the problem. The simulated annealing algorithm is a stochastic method that promises to find the global optimum in probability. In addition to strong robustness, it has other merits such as easy implementation and being suitable for large scale problems in that increasing the number of optimization parameters results in very small increase in computational time, which seems to be what genetic algorithms and other nongradient methods lack. The simulated annealing algorithm has not been applied in trajectory optimization so far. The application, if successful, will not only provide a badly needed alternative to the trajectory optimization problem for the aerospace plane, but will also establish a promising approach for other optimzation problems of nonsmooth dynamic systems.

3. 3-D Maneuvers

Our preceding work has revealed that the two constraints (8) and (9) severely restrict the flight envelop of the NASP in 2-D flight. The fuel-optimal ascent trajectory does not enjoy sinificant fuel saving as compared to a feasible trajectory that satisfies all the constraints. 3-D maneuvers may relax some of the restriction, thus offer better fuel

economy. Admittedly, 3-D optimal solutions will be even more difficult than the 2-D case. The investigation toward this direction necessitates a more robust optimization algorithm. The simulated annealing algorithm may help in this regard.

4. Adaptive Guidance

It has been observed that a set values for the guidance parameters that work very well for certain disturbances may not be the best choice for other disturbances. In fact, the ranges for the best choices of the guidance parameters for different disturbances that may be encountered in the flight of the aerospace plane may have no overlap. This suggests that an adaptive gain update scheme may remarkably improve the performance of the guidance system. Since the system dynamics is highly nonlinear, some new adaptive algorithm needs to be developed. The application of neural network to form a closed-loop adaptive mechanism for determining guidance parameters may prove attractive.

REFERENCES

[1] Lu, P., "Trajectory Optimization and Guidance for a Hypersonic Vehicle", AIAA paper 91-5068, Third AIAA International Aerospace Planes Conference, Orlando, FL, Dec. 3–5, 1991.

[2] Lu, P., "An Inverse Dynamics Approach to Trajectory Optimization and Guidance for an Aerospace Plane", AIAA paper 92-4331, to be presented at the Guidance, Navigation and Control Conference, Hilton Head, SC, August 10–12, 1992.

[3] Shaughnessy, J. D., Pinckey, S. Z., McMinn J. D., Cruz, C. I., and Kelley M-L., "Hypersonic Vehicle Simulation Model: Winged-Cone Configuration", NASA TM 102610, November 1990.

[4] Calise, A. J., Corban, J. E., and Flandro, G. A., "Trajectory Optimization and Guidance Law Development for National Aerospace Plane Applications", Final Report, NASA CR Number NAG-1-784, Dec., 1988.

[5] Vukobtatovic, M., and Stojic, R., *Modern Aircraft Flight Control*, Springer-Verlag, New York, 1988.

[6] Lane, S. H., and Stengel, R. F., "Flight Control Design Using Nonlinear Inverse Dynamics", Automatica, Vol. 24, No. 4, July, 1988, pp. 471–483.

[7] Hargraves C. R., and Paris S. W., " Direct Trajectory Optimization Using Nonlinear Programming and Collocation", AIAA Journal of Guidance, Control, and Dynamics, Vol. 10, No. 4, pp. 338–342, 1987.

[8] Pouliot, M. R., "CONOPT2: A Rapidly Convergent Constrained Trajectory Optimization Program for TRAJEX", Report N0. GDC-SP-82-008, General Dynamics, Convair Division, San Diego, CA, 1982.

[9] Findlay, J.T., Kelly, G.M., McConnell, J.G., and Compton, H.R., "Shuttle 'Chanllenger' Aerodynamic Performance From Flight Data Comparison with Predicted Values and 'Columbia' Experience", AIAA paper 84-0485, Jan., 1984.

[10] Calise, A. J., Corban, J. E., and Markopoulos, N., "Real Time Guidance and Propulsion Control For Aerospace Plane Applications", AIAA-91-5075, Third International Aerospace Planes Conference, Orlando, FL, 3–5, December, 1991.

[11] Bryson, A. E. and Ho, Y. C., *Applied Optimal Control: Optimization, Estimation, and Control*, Hemisphere Press, New York, 1975.

[12] Jacobson, D. H.,"Totally Singular Quadratic Minimization Problems", IEEE Transactions on Automatic Control, Vol. AC-16, NO.6, 1971.

[13] Gilbert, E. G., Howe, R. M., Lu, P. and Vinh, N. X., "Optimal Aeroassisted Intercept Trajectories At Hyperbolic Speeds", *AIAA Journal of Guidance, Control, and Dynamics*, Vol. 14, No. 1, Jan.–Feb., 1991, pp. 123–131.

[14] Belisle, C. J. P., Romeijn, H. E., Smith, R. L., "Hide-and-Seek: A Simulated Annealing Algorithm for Global Optimization", Technical Report No. 90-25, Department of Industrial and Operations Engineering, the University of Michigan, Ann Arbor, MI, September, 1990.

APPENDIX

Singular Rocket Thrust Control

The adjoint system to Eqs. (1), (3)–(5) is

$$\dot{p}_r = \frac{p_v}{m}\frac{\partial D}{\partial r} - \frac{2p_v\mu\sin\gamma}{r^3} - p_\gamma(-\frac{v}{r^2} + \frac{2\mu}{vr^3})\cos\gamma \qquad (A1)$$

$$\dot{p}_v = -p_r\sin\gamma + \frac{p_m}{m}\frac{\partial D}{\partial v} - \frac{p_vT\sin\varepsilon}{mv^2} - p_\gamma(\frac{1}{r} + \frac{\mu}{v^2r^2})\cos\gamma \qquad (A2)$$

$$\dot{p}_\gamma = -p_rv\cos\gamma + p_v\frac{\mu\cos\gamma}{r^2}$$
$$+ p_\gamma(\frac{v}{r} - \frac{\mu}{vr^2})\sin\gamma \qquad (A3)$$

$$\dot{p}_m = \frac{p_vT\cos\varepsilon}{m^2} - \frac{p_\gamma T\sin\varepsilon}{m^2v} - \frac{p_vD}{m^2} \qquad (A4)$$

On a singular arc, the switching function $S = 0$

$$S = vp_v\cos\varepsilon - p_\gamma\sin\varepsilon - \frac{mvp_m}{g_0I_{sp}} = 0 \qquad (A5)$$

$\partial H/\partial\varepsilon = 0$ leads to

$$vp_v\sin\varepsilon + p_\gamma\cos\varepsilon = 0 \qquad (A6)$$

The semi-positiveness of $\mathbf{H}_{uu}$ in Eq. (46) depends on the sign of

$$\frac{\partial H^2}{\partial\varepsilon^2} = -vp_v\cos\varepsilon + p_\gamma\sin\varepsilon \qquad (A7)$$

With Eqs. (A5) and (A6), Eq. (A7) is equivalent to

$$\frac{\partial H^2}{\partial\varepsilon^2} = -\frac{mp_mv}{g_0I_{sp}} \qquad (A8)$$

which is Eq. (42). As pointed in the paper, $p_m < 0$. In particular, if $D = 0$ and the final arc is singular, using Eqs. (A4)–(A6) and $p_m(t_f) = -1$ results in

$$m(t)p_m(t) = \text{constant} = -m(t_f)$$

For minimum-fuel problem with free end time, the Hamiltonian $H = 0$ (Eq. (37)). On a singular arc, we also have

$$H - TS = p_rv\sin\gamma - p_v(\frac{D}{m} + \frac{\sin\gamma}{r^2})$$
$$+ p_\gamma(\frac{v}{r} - \frac{\mu}{vr^2})\cos\gamma = 0 \qquad (A9)$$

39

Differentiating (A9) twice and after much algebraic operation, we obtain for $z = \tan(\varepsilon/2)$

$$Az^4 + Bz^3 + Cz^2 + Ez + F = 0 \qquad (A10)$$

where

$$A = \sin\gamma\left(\frac{D}{mv^2} - \frac{D}{mvg_0I_{sp}} - \frac{\mu\sin\gamma}{r^2v^2}\right)$$

$$B = -2\left(\frac{\mu\sin 2\gamma}{r^2v^2} + \frac{D\cos\gamma}{mv^2}\right)$$

$$C = \frac{4}{r} + \frac{2D\sin\gamma}{mv^2} - \frac{4\mu\cos^2\gamma}{r^2v^2} + \frac{2\mu\sin^2\gamma}{r^2v^2} \qquad (A11)$$

$$E = -B$$

$$F = \sin\gamma\left(\frac{D}{mv^2} + \frac{D}{mvg_0I_{sp}} - \frac{\mu\sin\gamma}{r^2v^2}\right)$$

When the final orbit is circular, the above conditions can be used to establish that *singular arc is not fuel-optimum solution for the portion of the trajectory immediately before orbital insertion*. We show this by contradiction. Assuming that the last optimal arc is singular, substituting orbital insertion conditions (7) in Eq. (A9) gives

$$\frac{p_v(t_f)D}{m(t_f)} = 0 \implies p_v(t_f) = 0 \text{ since } D \neq 0 \qquad (A12)$$

Also combining conditions (9), (A10) and (A11) produces

$$\varepsilon(t_f) = 0 \qquad (A13)$$

Then Eqs. (A5), (A12) and A(13) give rise to

$$p_m(t_f) = 0 \qquad (A14)$$

which is contradictory to the transversality condition $p_m(t_f) = -1$. So singular arc is not optimal. On the other hand, since at the orbital altitude drag D is very small, a coast arc cannot achieve circular orbital insertion for any reasonable length of time (In particular, if $D = 0$, circular orbital insertion is impossible by coasting). In conclusion, the final arc of a fuel-optimal trajectory must be full-throttle.